

Composition dependence of hardness and elastic modulus of the cubic and hexagonal NbCo₂ Laves phase polytypes studied by nanoindentation

Wei Luo^{1,a)}, Christoph Kirchlechner¹, Juan Li¹, Gerhard Dehm¹, Frank Stein^{1,b)}

¹Max-Planck-Institut für Eisenforschung GmbH, Department of Structure and Nano-/Micromechanics of Materials, D-40237 Düsseldorf, Germany

^{a)}Address all correspondence to these authors. e-mail: weiluomse@hotmail.com, w.luo@mpie.de

^{b)}e-mail: stein@mpie.de

Received: 22 August 2019; accepted: 27 November 2019

Regarding the effect of composition on the mechanical properties of intermetallic phases such as Laves phases, there is conflicting information in the literature. Some authors observed defect hardening when deviating from stoichiometric Laves phase composition, whereas others find defect softening. Here, we present a systematic investigation of the defect state, hardness, and elastic modulus of cubic and hexagonal NbCo₂ Laves phases as a function of crystal structure and composition. For this purpose, diffusion couples were prepared which exhibit diffusion layers of the cubic C15 and hexagonal C14 and C36 NbCo₂ Laves phases, with concentration gradients covering their entire homogeneity ranges from 24 to 37 at.% Nb. Direct observations of dislocations and stacking faults in the diffusion layers as a function of composition were performed by electron channeling contrast imaging, and the hardness and elastic modulus were probed in the diffusion layers along the concentration gradients by nanoindentation.

Introduction

Laves phases constitute one of the largest classes of intermetallic phases, and some of them are promising candidates for high-temperature applications because of their high melting points combined with high strength and good creep resistance [1]. However, the knowledge of their mechanical properties is still limited, and the effect of composition and crystal structure on their mechanical properties is not understood yet. A particularly well-suited Laves phase to study this issue is NbCo₂ as it exists as a stable phase in a wide composition range between 24 and 37 at.% Nb, where its crystal structure type changes with increasing Nb content from hexagonal C36 to cubic C15 above 25 at.% Nb and finally to the hexagonal C14 variant existing between 35.5 and 37 at.% Nb [2]. Regarding the effect of composition on the hardness of NbCo₂, there is a strong controversy in the literature. Liu and Zhu et al. [3, 4] report that the Vickers hardness of NbCr₂, NbFe₂, and NbCo₂ increases as the composition deviates from the stoichiometric value. They proposed that the increase in hardness on both sides of the stoichiometric composition is because of the hardening effect of antisite defects existing at off-

stoichiometric compositions. On the contrary, Voß et al. [5] report that the Vickers hardness of the NbFe₂ and NbCo₂ Laves phase has a maximum at the stoichiometric composition and decreases as the composition deviates from the stoichiometric composition, indicating defect softening. A big issue that might explain the different findings is the difficulty of producing bulk, single-phase Laves phase alloys. Although a dedicated method described by Voß et al. [6] was used to produce Laves phase alloys, there are still certain amounts of second phases, impurities, pores, and microcracks inside the alloys. These factors may lead to large scatter in the Vickers hardness and make it difficult to judge about the real compositional trend of the hardness. Voß [7] also studied the composition dependence of elastic properties of Laves phases. He reports that Young's modulus of the NbFe₂ and NbCo₂ Laves phases decreases as the composition deviates from the stoichiometric composition, which is consistent with the results for HfCo₂ reported by Chen et al. [8].

To circumvent difficulties in preparing a series of flawless bulk Laves phase alloys and systematically study the influence of composition and crystal structure on the hardness and elastic modulus of the NbCo₂ Laves phase, we follow a different strategy

in the present work. It has been demonstrated that the combination of diffusion couples and microscale property measurements is a powerful tool to efficiently map composition–structure–property data [9]. Here, the diffusion couple technique is used to grow diffusion layers of the C14, C15, and C36 NbCo₂ Laves phases. With this method, the same heat treatment and preparation procedures can be maintained for all the Laves phases. As there are continuous concentration gradients in the diffusion layers, the hardness and the elastic modulus as a function of composition can be probed in the diffusion layers along the concentration gradients by nanoindentation. In addition, the electron channeling contrast imaging (ECCI) technique, which is a powerful tool for detecting crystal defects [10], was used for the direct observation of dislocations and stacking faults in the diffusion layers of the cubic and hexagonal NbCo₂ Laves phases as a function of composition.

Experimental results

Microstructures and concentration profiles of the diffusion couples

Figures 1(a) and 1(b) show the microstructures of the Co/Co–30Nb and Nb/Co–30Nb diffusion couple after annealing at 1200 °C for 96 h and Nb/Co–30Nb diffusion couple after annealing at 1350 °C for 24 h, respectively. To identify the diffusion zones of different types of NbCo₂ Laves phase, the diffusion couples were analyzed by electron backscatter diffraction (EBSD). Figures 1(c) and 1(d) show the color-coded EBSD orientation maps of the diffusion zones of the cubic and hexagonal NbCo₂ Laves phases. The corresponding concentration profiles are given in Figs. 1(e) and 1(f), respectively.

Co/Co–30Nb diffusion couple exhibits a diffusion layer of C36 NbCo₂ with a thickness of about 70 μm and an extended diffusion zone of C15 NbCo₂ with a thickness of 400 μm. Nb/

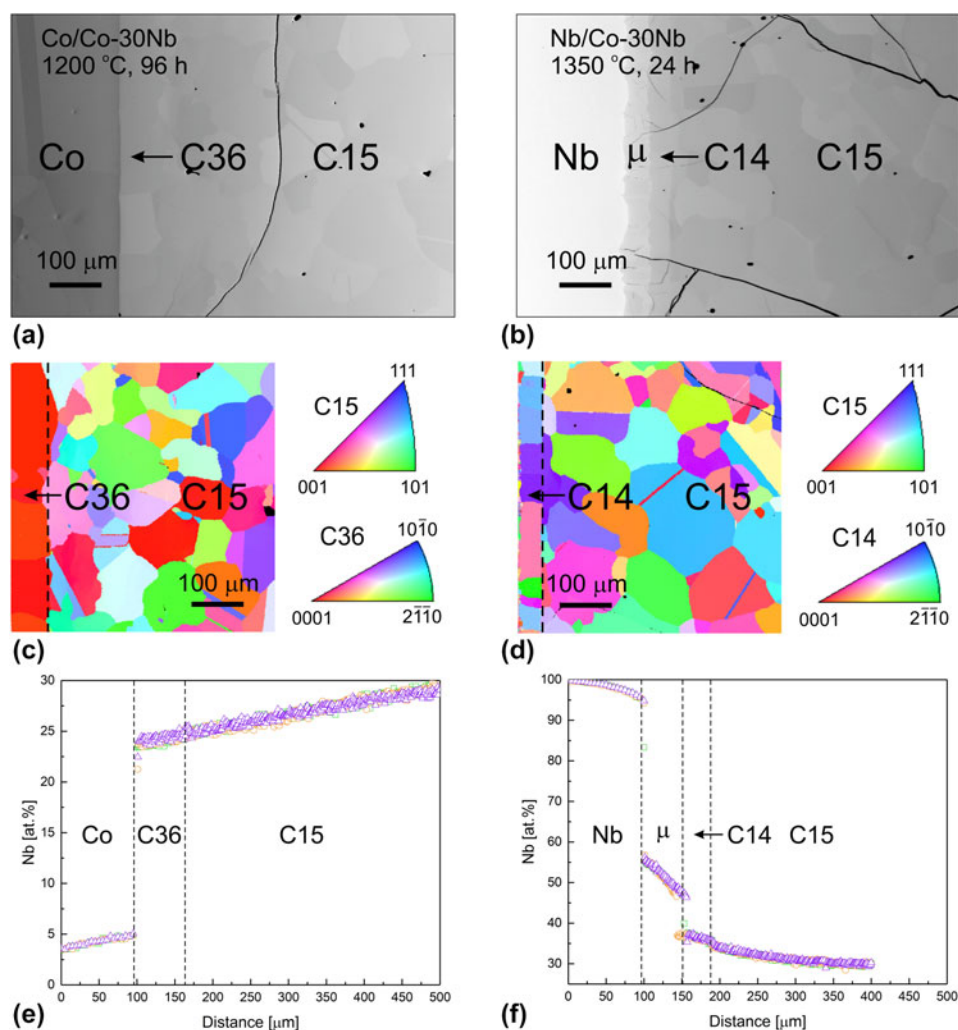


Figure 1: Microstructures of the (a) Co/Co–30Nb and (b) Nb/Co–30Nb diffusion couples, color-coded EBSD mapping of crystallographic orientations of the cubic and hexagonal NbCo₂ Laves phases in the (c) Co/Co–30Nb and (d) Nb/Co–30Nb diffusion couple and concentration profiles of the (e) Co/Co–30Nb and (f) Nb/Co–30Nb diffusion couples. The concentration profiles were measured perpendicular to the interfaces of the diffusion layers by EPMA scans. Three EPMA scans were measured for each diffusion couple. The differently colored and shaped symbols in the concentration profiles represent data obtained from different EPMA scans.

Co–30Nb diffusion couple contains a diffusion layer of C14 NbCo₂ and an extended diffusion zone of C15 NbCo₂ with thicknesses of 40 and 200 μm, respectively. Grain sizes in the three Laves phase layers are in the 100 μm range. The homogeneity ranges of C36 and C14 NbCo₂ obtained from the diffusion couples are approximately 24.0 ± 0.5 to 25.0 ± 0.5 at.% Nb and 35.5 ± 0.5 to 37.0 ± 0.5 at.% Nb, respectively. Although the two hexagonal NbCo₂ Laves phases exist in a narrow composition range, the cubic C15 NbCo₂ Laves phase is stable in a wide composition range from 25.0 ± 0.5 to 34.3 ± 0.5 at.%. The error bars of the composition values are maximum errors determined from the concentration profiles. The existence of the three structure types of the NbCo₂ Laves phase and their measured homogeneity ranges are in agreement with Stein et al. [2].

ECCI observation of defects

The C15 NbCo₂ Laves phase in the Co/Co–30Nb diffusion couple reveals only a few dislocations in ECCI images at positions far away from the interface between C15 and C36 NbCo₂ [see Fig. 2(a)]. The composition measured in this area by electron probe microanalysis (EPMA) is about 30 at.% Nb. On average, the dislocation density in the C15 NbCo₂ Laves phase at 30 at.% Nb is measured to be $6 \pm 3 \times 10^{11} \text{ m}^{-2}$. The dislocation density was measured from 5 different grains. The error bar represents the standard deviation.

ECCI was performed in different areas of the diffusion couples along the concentration gradient. The C15 NbCo₂ Laves phase in a composition range from about 26 to 34 at.% shows individual dislocations, and the dislocation density remains on an approximately constant level. However, a high

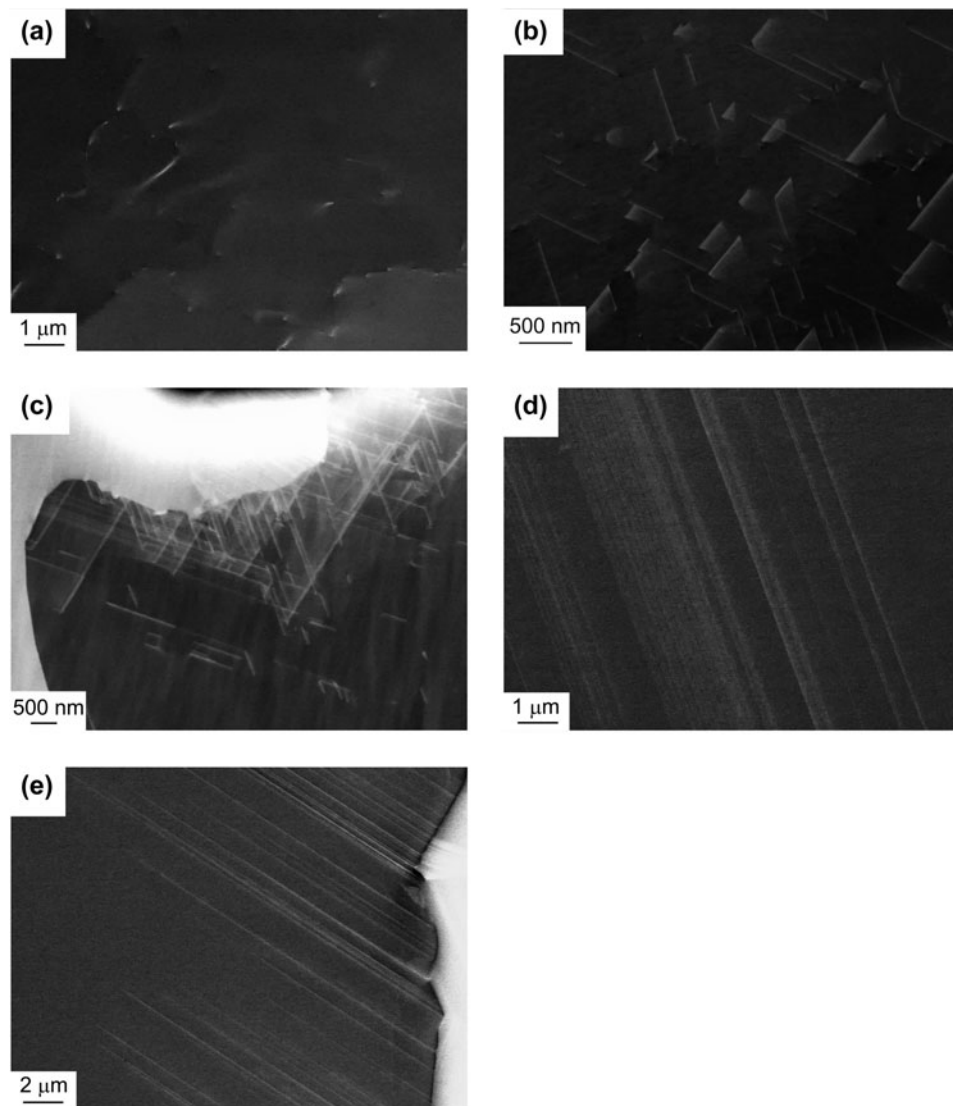


Figure 2: ECC images of (a) C15 NbCo₂ at 30 at.% Nb, (b) C15 NbCo₂ at 25 at.% Nb (Co-rich phase boundary), (c) C15 NbCo₂ at 34.3 at.% Nb (Nb-rich phase boundary), (d) C36 NbCo₂ at 24.5 at.% Nb, and (e) C14 NbCo₂ at 36 at.% Nb taken from the diffusion couples.

density of widely extended stacking faults occur in C15 NbCo₂ close to the Co-rich phase boundary [Fig. 2(b)], where the composition is about 25 at.% Nb. The width of the stacking faults can be as large as several micrometers, and they are lying on crystallographic {111} planes. The dislocation density of C15 NbCo₂ at the Co-rich phase boundary is estimated to be $4 \pm 2 \times 10^{12} \text{ m}^{-2}$. Similarly, a high density of extended stacking faults were also observed in C15 NbCo₂ close to the Nb-rich phase boundary [Fig. 2(c)], where the composition is about 34.3 at.% Nb. Here, the average dislocation density of C15 NbCo₂ is determined to be $5 \pm 2 \times 10^{12} \text{ m}^{-2}$. Generally, while C15 NbCo₂ reveals only few dislocations (in the order of 10^{11} m^{-2}) in a composition range from 26 to 34 at.% Nb, the dislocation density of C15 NbCo₂ at the Co- and Nb-rich phase boundaries is about one order of magnitude higher. The occurrence of widely extended stacking faults at the Co- and Nb-rich phase boundaries of C15 NbCo₂ indicates the stacking fault energy (SFE) of C15 NbCo₂ decreases significantly at the boundaries of its homogeneity range. As shown in Figs. 2(d) and 2(e), stacking faults with tens of micrometers in width were observed in the diffusion layers of the C36 and C14 NbCo₂ Laves phases.

In the NbCo₂ alloy with 25.6 at.% Nb [Fig. 3(a)], C15 NbCo₂ exhibits wide stacking faults lying on {111} planes, whereas the C15 NbCo₂ alloy with 30 at.% Nb [Fig. 3(b)] shows only a few dislocations and low-angle grain boundaries. High

densities of planar defects on the basal plane extending across the whole grains were observed in the alloys of C36 [Fig. 3(c)] and C14 NbCo₂ [Fig. 3(d)]. These observations are in agreement with the findings from the diffusion couples.

Hardness and elastic modulus measured by nanoindentation

As shown in Figs. 4(a) and 4(b), a series of nanoindentation tests were performed in diffusion zones of the cubic and hexagonal NbCo₂ Laves phases in the Co/Co-30Nb and Nb/Co-30Nb diffusion couples. No cracks were observed originating from the indents. The hardness and elastic modulus of the cubic and hexagonal NbCo₂ Laves phases as a function of the composition are shown in Figs. 5(a) and 5(b), respectively. The hardness of C15 NbCo₂ at the stoichiometric composition is $14.7 \pm 0.3 \text{ GPa}$ and remains unchanged between 28 and 34 at.% Nb within the given accuracy. As the composition approaches the Co-rich phase boundary, the hardness of C15 NbCo₂ decreases from $14.5 \pm 0.2 \text{ GPa}$ at 28 at.% Nb to $13.7 \pm 0.4 \text{ GPa}$ at 25 at.% Nb. The hardness of the C36 NbCo₂ phase at 24.5 at.% Nb is $13.4 \pm 0.3 \text{ GPa}$, and the average hardness of C14 NbCo₂ at 36 at.% Nb is $14.3 \pm 0.3 \text{ GPa}$. The compositional dependency of the elastic modulus is similar to that of the hardness. The elastic modulus of C15 NbCo₂ at the stoichiometric composition is $290 \pm 8 \text{ GPa}$ and remains nearly constant between 26 and 34 at.% Nb. At 25 at.% Nb, the

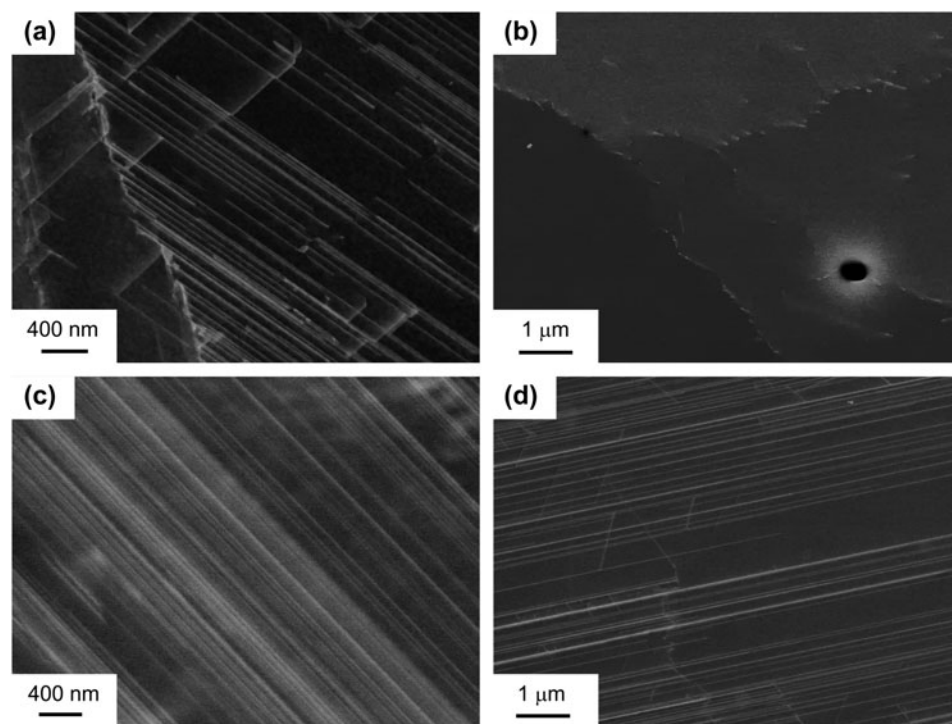


Figure 3: ECC images of (a) C15 NbCo₂ at 25.6 at.% Nb, (b) C15 NbCo₂ at 30 at.% Nb, (c) C36 NbCo₂ at 25.1 at.% Nb, and (d) C14 NbCo₂ at 36 at.% Nb taken from the NbCo₂ alloys.

elastic modulus of C15 NbCo₂ decreases to 281 ± 9 GPa. The respective values of the elastic modulus of C36 NbCo₂ at 24.5 at.% Nb and C14 NbCo₂ at 36 at.% Nb are 273 ± 4 and 261 ± 8 GPa. These values are about 6% and 10% lower than for C15 NbCo₂ at the stoichiometric composition, respectively.

In Fig. 6, the hardness values of the cubic C15 and hexagonal C14 and C36 NbCo₂ Laves phase alloys measured in various orientations are shown in the inverse pole figures. It can be seen that the hardness values of the C15 NbCo₂ alloys with 25.6 at.% [Fig. 6(b)] and 33 at.% Nb [Fig. 6(c)] are independent of orientation within the given accuracy. The hardness of C36 NbCo₂ [Fig. 6(a)] also appears to be independent of the orientation, whereas for the C14 NbCo₂ Laves phase [Fig. 6(d)], the hardness measured perpendicular to the basal plane is slightly higher (in the order of 5%) than in the other orientations. In accordance with the results from the diffusion couples, the hardness of C36 NbCo₂ at 25 at.% Nb and C14 NbCo₂ at 36 at.% is lower than that of C15 NbCo₂ and the hardness of C15 NbCo₂ decreases as the composition approaches the Co-rich phase boundary.

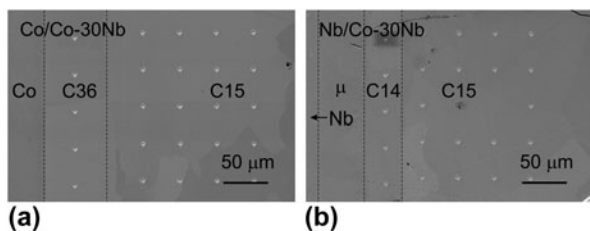


Figure 4: SEM images showing the indents in the diffusion zones of the cubic and hexagonal NbCo₂ Laves phases in the diffusion couples (a) Co/Co-30Nb and (b) Nb/Co-30Nb.

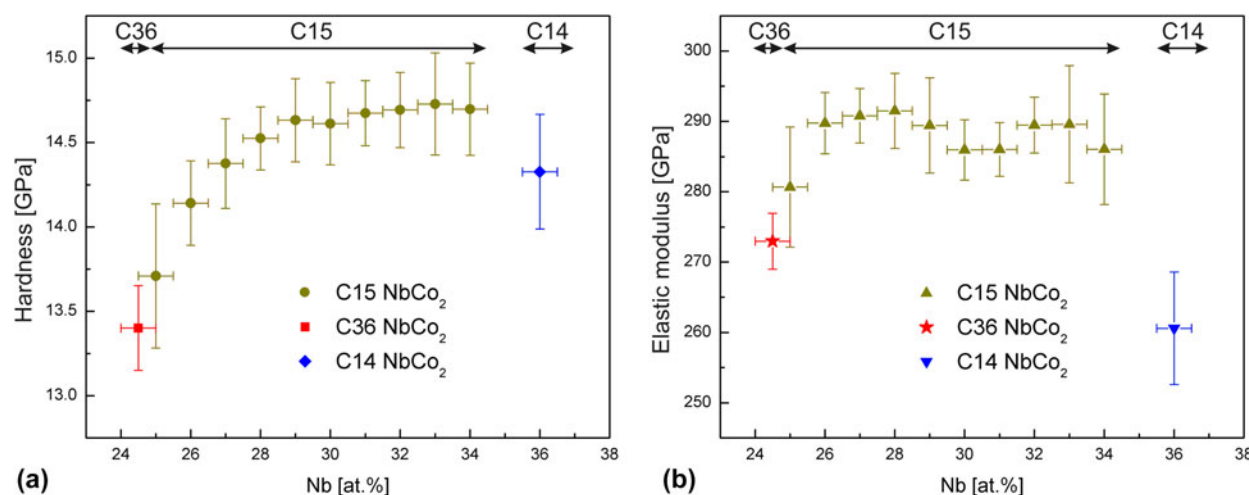


Figure 5: (a) Hardness and (b) elastic modulus of the cubic and hexagonal NbCo₂ Laves phases measured from the diffusion couples as a function of composition. At least 15 indents were made for each composition. The error bars of the hardness and elastic modulus represent the standard deviations of the measured data. The compositions of the indents are determined according to their distances to the interface and the concentration profiles of the two diffusion couples [see Figs. 1(e) and 1(f)]. The error bars of the compositions represent the maximum and minimum composition values at the corresponding positions determined from the concentration profiles.

Discussion

Effect of composition on the defect state

The dislocation density in Laves phases in the as-cast state is known to be generally very low compared with other metallic alloys. The average dislocation density of as-cast NbCr₂ and MgZn₂ was reported to be about $5 \times 10^5 \text{ m}^{-2}$ [11] and 10^{11} m^{-2} [12], respectively. However, in cases such as NbCo₂ where a change in chemical composition can lead to a phase transformation between different structure types, a change in the defect state and density could occur as the composition approaches the phase boundaries between the different structure types. Takata et al. [13] reported that whereas the binary C14 Fe-27Nb (at.% Nb) Laves phases exhibit only few dislocations, a high density of widely extended planar defects occur in the ternary C14 Fe-26Nb-33Ni (at.% Nb) Laves phase, which is close to the Ni-rich boundary probably because of a decrease in the stability of the C14 structure toward other hexagonal polytypes such as 4H and 6H structures [13]. Another example is the Hf-V-Nb system [14], where the C14 and C15 Laves phases exist as stable phases in two adjacent phase fields. Luzzi et al. [14] reported that an increase of stacking fault density was observed in the C15 Hf-V-Nb Laves phase as the composition approaches the homogeneity range of the adjacent C14 polytype. The occurrence of the stacking faults in the C15 Hf-V-Nb Laves phase indicates a decrease in the SFE of the C15 Hf-V-Nb Laves phase at the phase boundary close to the C14 variant. It has been confirmed by high resolution transition electron microscopy that the stacking faults observed at the phase boundaries of the C15 Hf-V-Nb Laves phase are of intrinsic character and the stacking sequence is similar to that of the C14 structure [14].

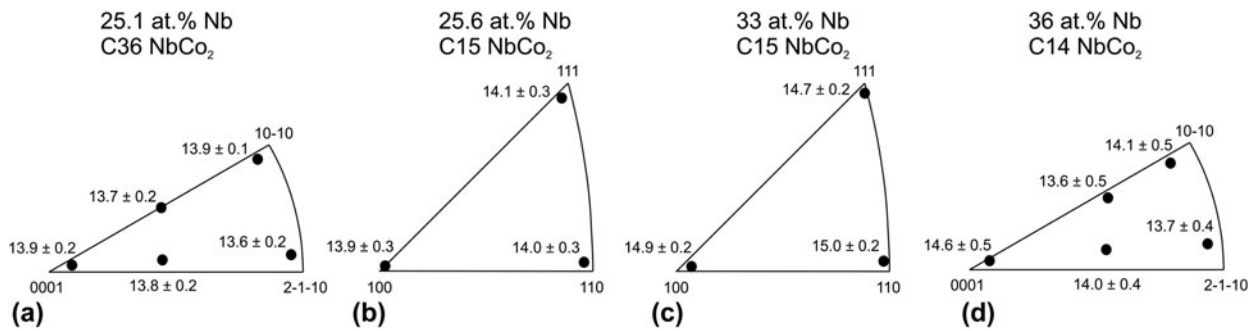


Figure 6: Hardness of (a) C36 NbCo₂ at 25.1 at.% Nb, (b) C15 NbCo₂ at 25.6 at.% Nb, (c) C15 NbCo₂ at 33 at.% Nb, and (d) C14 NbCo₂ at 36 at.% Nb measured from the NbCo₂ alloys in various orientations.

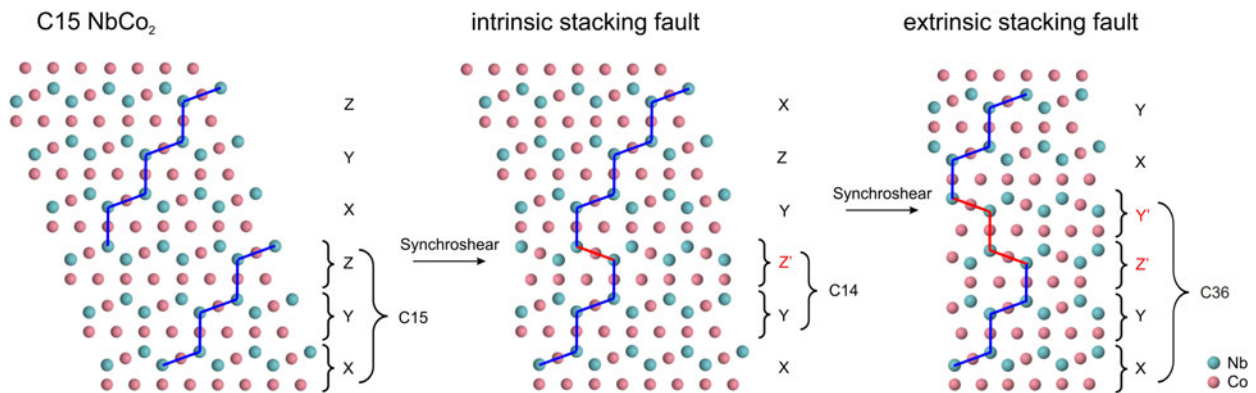


Figure 7: Schematic illustration of the formation of an intrinsic and an extrinsic stacking fault in the C15 structure. X, Y, and Z represent the quadruple layers in Laves phases, and X', Y', and Z' are the respective twin-related quadruple layers [15]. The stacking faults are marked in red. Similar to the formation of stacking faults in the C14 Laves phase [16], intrinsic and extrinsic stacking faults in the C15 structure can also be formed through the synchroshear mechanism. As the YZ' stacking is identical to the stacking of the C14 structure, an intrinsic stacking fault can be seen as a layer of the C14 structure, resulting from phase transformation of the C15 structure. Similarly, as the XYZ'Y' stacking is identical to that of the C36 structure, an extrinsic stacking fault can be seen as a layer of the C36 structure.

As described earlier, the present ECCI observations reveal that the C15 NbCo₂ Laves phase exhibits only a few individual dislocations in the composition range from 26 to 34 at.% Nb, whereas at the boundaries close to the hexagonal variants, that is, at about 25.0 at.% Nb and 34.3 at.% Nb, a high density of stacking faults are present in C15 NbCo₂. These findings are consistent with the results reported for other Laves phases [13, 14].

The crystal structures of Laves phases are usually described as a certain stacking sequence of a fundamental, 4-layered structural unit (X, Y, and Z) which is composed of a single layer of small atoms (A, B, and C) and a sandwiched triple layer ($\alpha\beta$, $\beta\alpha\gamma$, and $\gamma\beta\alpha$) containing two layers of large atoms separated by a layer of small atoms [15]. The X', Y', and Z' quadruple layers are twin-related to the respective X, Y, and Z counterparts. Similar to the formation of stacking faults in the C14 Laves phase [16], intrinsic and extrinsic stacking faults in the C15 structure can also form through the synchroshear mechanism. As shown in Fig. 7, the stacking sequence of the C15 structure is XYZ. A synchro-Shockley partial dislocation glides through a Z layer and changes the Z layer to Z'. The local stacking sequence becomes XYZ'YZ, and an intrinsic stacking fault is formed as indicated by the

“missing” X layer. As the YZ' stacking is identical to the stacking of the C14 structure, the intrinsic stacking fault can also be seen as a layer of the C14 structure resulting from phase transformation of the C15 structure. If another synchro-Shockley partial dislocation on the adjacent plane glides through the Y layer above the Z' layer, the Y layer becomes Y' and the local stacking sequence is XYZ'Y', which is identical to the stacking sequence of the C36 structure. An additional layer of Y' is inserted between the Z' layer and X layer, indicating an extrinsic stacking fault. An intrinsic stacking fault and an extrinsic stacking fault in the C15 structure can be considered as a thin layer of the C14 and C36 Laves phases, respectively. Therefore, the SFE of the intrinsic and extrinsic stacking faults can be estimated from the energy difference between C15 and C14 and between C15 and C36, respectively. Chu et al. [17] proposed an equation to estimate the intrinsic SFE:

$$\gamma_{\text{ISF}} = \frac{24\Delta\epsilon_{\text{C15-C14}}}{3^{1/2}a^2} \quad (1)$$

where γ_{ISF} is the intrinsic SFE, $\Delta\epsilon_{\text{C15-C14}}$ is the energy difference between the C15 and C14 structure, a is the lattice

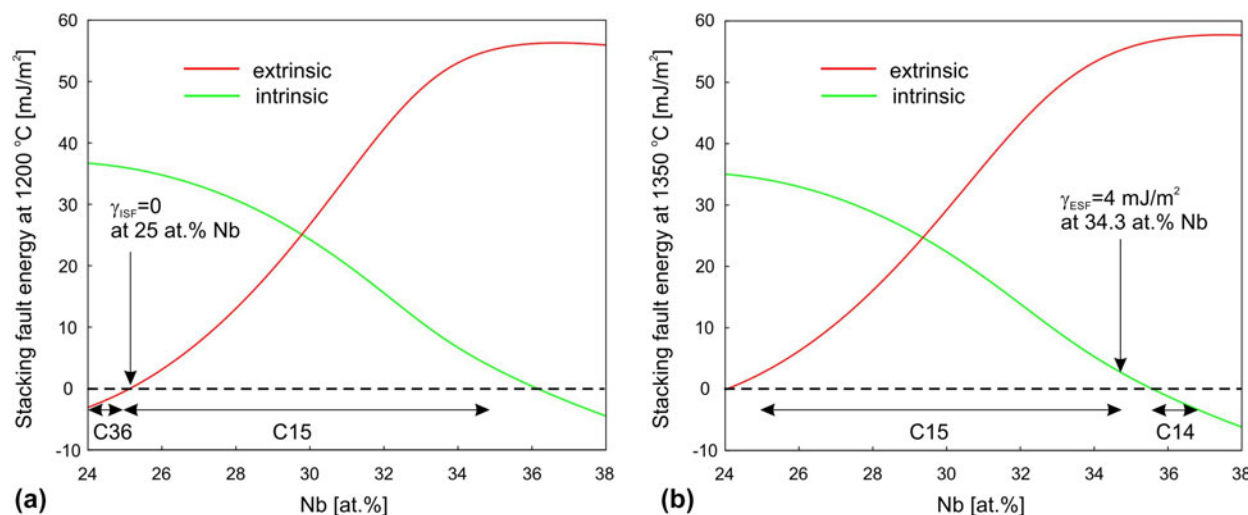


Figure 8: Calculated intrinsic (i.e., C14-like) and extrinsic (i.e., C36-like) SFE of the C15 NbCo₂ Laves phase at (a) 1200 °C and (b) 1350 °C as a function of composition.

parameter of the C15 Laves phase. Similarly, Sun and Jiang [18] reported an equation to calculate the extrinsic SFE:

$$\gamma_{\text{ESF}} = \frac{48\Delta\epsilon_{\text{C15-C36}}}{3^{1/2}a^2} \quad (2)$$

where γ_{ESF} is the extrinsic SFE, $\Delta\epsilon_{\text{C15-C36}}$ is the energy difference between the C15 and C36 structure, and a is the lattice parameter of the C15 Laves phase.

The energy differences between the Laves phases can be calculated from the Gibbs energy functions of the C14, C15, and C36 NbCo₂ Laves phases, which are available from He et al. [19]. They performed thermodynamic modeling of the Co–Nb system on the basis of data from experimental phase diagram studies and ab initio calculations. Based on the thermodynamic parameters provided by He et al. [19], the intrinsic and extrinsic SFE for the C15 NbCo₂ Laves phase as a function of composition at 1200 °C [Fig. 8(a)] and 1350 °C [Fig. 8(b)] was obtained. These temperatures were chosen as the Co/Co–30Nb and Nb/Co–30Nb diffusion couples were heat treated at 1200 and 1350 °C, respectively. The extrinsic and intrinsic SFE of C15 NbCo₂ is relatively low, which is consistent with the very small differences in the total energy of the three NbCo₂ Laves phase polytypes [20]. In the composition range between about 24 and 30 at.% Nb, the extrinsic SFE is lower than the intrinsic SFE, which indicates the formation of extrinsic (i.e., C36-like) stacking faults in C15 NbCo₂ is energetically more favorable on the Co-rich side. In Fig. 8(a), at 1200 °C, the extrinsic SFE decreases as the Nb content decreases and becomes 0 at 25 at.% Nb, which is the Co-rich boundary of the homogeneity range of C15 NbCo₂. This suggests that at 25 at.% Nb, extrinsic stacking faults with extremely large width, that is, C36-like ordered layer stacks, can be readily formed. By contrast, the intrinsic SFE is lower than

the extrinsic SFE in the Nb-rich composition range between about 30 and 37 at.% Nb, indicating that stacking faults in Nb-rich C15 NbCo₂ can be expected to be of intrinsic (i.e., C14-like) character. Figure 8(b) shows that at 1350 °C, the intrinsic SFE decreases as the Nb content increases. At 34.3 at.% Nb, the calculated intrinsic SFE is already very low (4 mJ/m²), explaining the occurrence of stacking faults in C15 NbCo₂ near its Nb-rich phase boundary in the Nb/Co–30Nb diffusion couple.

Effect of composition on the hardness and elastic modulus

Chen et al. [21] calculated the elastic properties of a series of transition metal Laves phases with the C15 structure by first-principles calculations. They reported that the calculated Young’s modulus of C15 NbCo₂ is 293.4 GPa, which is in reasonable agreement with the present results ranging from 281 to 290 GPa depending on the composition. In the present work, the elastic modulus of C15 NbCo₂ is nearly constant from 26 to 34 at.% Nb. However, at 25 at.% Nb, where the SFE decreases and a high density of stacking faults occur, the elastic modulus of C15 NbCo₂ decreases. This decrease in modulus of C15 NbCo₂ at the Co-rich phase boundary could be related to the reduced thermodynamic phase stability of the C15 structure.

The hardness of C15 NbCo₂ is constant from 28 to 34 at.% Nb and decreases as the composition approaches the Co-rich phase boundary. Takata et al. [13] reported a similar behavior in the NbFe₂-based ternary Laves phase. They found that although the hardness of binary Fe–27Nb (at.% Nb) and the ternary Fe–27Nb–18Ni (at.% Nb) Laves phase is almost identical and independent of orientation, the hardness of ternary Fe–26Nb–33Ni (at.% Nb) Laves phase, which is located close to the Ni-rich phase boundary, is lower and exhibits anisotropic behavior.

Softening of Laves phases with deviation from the stoichiometric composition was reported by several authors [5, 8, 22], but the underlying mechanism is not clear yet. An example is the MgZn₂ Laves phase. As the composition deviates from the stoichiometric composition, a decrease in hardness and yield strength was observed accompanied by a reduction in the initial dislocation density [22, 23]. The softening effect is attributed to the decrease in the initial dislocation density at off-stoichiometric compositions [23]. The constitutional defects in Laves phases at off-stoichiometric compositions might also aid the deformation process and contribute to the softening effect [8, 24, 25]. Moreover, the softening of the Laves phase is also associated with the decrease in shear modulus at off-stoichiometric compositions [8]. However, the present results show that the hardness and elastic modulus of the NbCo₂ Laves phase are largely independent of the chemical composition, unless the composition approaches the Co-rich and Nb-rich phase boundaries, where C15 NbCo₂ transforms to C36 and C14 NbCo₂, respectively. This behavior cannot be well explained by the previous assumptions.

Because of the self-pinning character of synchro-Shockley dislocations in the Laves phases [26], the dislocation motion via the synchroshear mechanism [27] in Laves phases is hindered at low temperature, resulting in high Peierls stress of Laves phases [1]. According to Qiu et al. [28], the indentation hardness of materials with high Peierls stress is given by adding the contribution of the friction stress to that of dislocation hardening:

$$H = H_{\text{fric}} + MC\alpha\mu b \sqrt{\rho_s(\epsilon_{\text{rep}}) + \rho_{\text{GND}}(h)} \quad , \quad (3)$$

$$H_{\text{fric}} = MC\tau_p \quad , \quad (4)$$

where H is the indentation hardness at a certain indentation depth h , H_{fric} is the contribution of the friction stress, M is the Taylor factor which relates the shear stress to the normal stress, C is the Tabor factor which converts the equivalent flow stress to hardness, α is a constant taken to be 0.5 in the calculations, τ_p is the Peierls stress, $\rho_s(\epsilon_{\text{rep}})$ is the density of statistically stored dislocations (SSDs) at a certain representative strain, $\rho_{\text{GND}}(h)$ is the density of geometrically necessary dislocations (GNDs) at the corresponding indentation depth h , μ is the shear modulus, and b is the magnitude of the Burgers vector of a perfect dislocation. According to Durst et al. [29], by considering the plastically deformed volume underneath the indenter and introducing a factor f , the density of GNDs is calculated as:

$$\rho_{\text{GND}}(h) = \frac{3 \tan^2 \theta}{2f^3 bh} \quad , \quad (5)$$

where θ is the angle between the surface and the indenter, and f is a factor which relates the contact radius and the radius of the

plastic zone. A Berkovich diamond indenter ($\tan \theta = 0.358$ [30]) was used, and the indentation depth is about 400 nm for all the indents. The Burgers vector of a perfect dislocation in C15 NbCo₂ has a length of 0.4778 nm, and the constant f is assumed to be 2.2 for a Berkovich indenter [29]. According to Eq. (5), the density of GNDs is calculated to be $9.4 \times 10^{13} \text{ m}^{-2}$. In the present work, the initial SSD density of the C15 NbCo₂ Laves phase in the bulk and close to the phase boundaries is in the order of 10^{11} and 10^{12} m^{-2} , respectively, which is significantly lower than the density of GNDs. Therefore, for the indentation depth of 400 nm, GNDs likely dominate the dislocation density. Assuming a Taylor factor $M = 3$ and a Tabor factor $C = 3$ [29], the contribution of dislocation hardening in hardness is about 2.4 GPa according to Eq. (3). The contribution of dislocation hardening is less than one-fifth of the total hardness of the cubic and hexagonal NbCo₂ Laves phases. This suggests that the hardness of the NbCo₂ Laves phase is mainly dominated by the high Peierls stress.

At the stoichiometric composition, the hardness of C15 NbCo₂ measured from nanoindentation is 14.7 GPa. The contribution of the Peierls stress to the hardness is estimated to be 12.3 GPa by subtracting the contribution of dislocation hardening from the measured hardness value. Thus, according to Eq. (4), the Peierls stress τ_p is calculated to be 1.4 GPa assuming $M = 3$ and $C = 3$. The Peierls stress of the $\frac{1}{6}\langle 11\bar{2} \rangle$ -type partial dislocation of C15 NbCr₂ [31] obtained by ab initio calculations ranges from 0.4 to 7.2 GPa, depending on the character of dislocation. The respective value for C15 HfCr₂ [31] ranges from 0.7 to 5.6 GPa. The estimated Peierls stress for C15 NbCo₂ of 1.4 GPa is in reasonable agreement with these reported values for C15 NbCr₂ and C15 HfCr₂.

According to Wang [32], the Peierls stress for edge and screw dislocation is $\tau_{\text{edge}} = \frac{\mu}{1-\nu} \exp(-\frac{4\pi\varsigma}{b})$ and $\tau_{\text{screw}} = \mu \exp(-\frac{4\pi\varsigma}{b})$, respectively. Here, ς is the half-width of the dislocation core. According to this model, the magnitude of the Peierls stress is determined by the geometrical configuration of the dislocation core and the bonding strength [33]. As the shear modulus decreases at the Co-rich and Nb-rich boundaries of the homogeneity range of the NbCo₂ Laves phase, the Peierls stress of NbCo₂ is expected to decrease at these compositions, leading to a decrease in hardness. However, as the dislocation core of the synchro-Shockley partial dislocation in Laves phases spreads on two adjacent planes, the accuracy of the prediction of Peierls stress using the this model is subjected to large errors [33]. Liu et al. [31] calculated the Peierls stress of C15 NbCr₂ and C15 HfCr₂ and the influence of the addition of a third element on the Peierls stress by ab initio calculations. It is shown that the substitution of a third element in C15 NbCr₂ and C15 HfCr₂ can change the dislocation core width and influence the Peierls stress. This suggests that the

constitutional defects of NbCo₂ at off-stoichiometric compositions might also affect the Peierls stress by changing the dislocation core width. Further ab initio calculations of the influence of the constitutional defects on the dislocation core structure and Peierls stress of the NbCo₂ Laves phase could help shed more light on the effect of composition on the hardness.

Conclusions

In the present work, extended diffusion layers of the cubic C15 and hexagonal C14 and C36 NbCo₂ Laves phases with concentration gradients covering the entire homogeneity ranges of these phases were prepared by the diffusion couple technique. Applying ECCI, the influence of composition on the defect state and density in the cubic and hexagonal NbCo₂ Laves phases was studied in detail. The hardness and elastic modulus as a function of composition were probed in the diffusion zones of the C14, C15, and C36 NbCo₂ Laves phases by nanoindentation. The following main conclusions can be drawn:

- (1) The elastic modulus of C14 and C36 NbCo₂ is lower than that of C15 NbCo₂. In the composition range of C15 NbCo₂, the elastic modulus remains nearly constant between 26 and 34 at.% Nb but clearly decreases at the Co-rich phase boundary, where the composition is about 25 at.% Nb. The decrease in the elastic modulus of C15 NbCo₂ at the Co-rich phase boundary could be related to the reduced thermodynamic phase stability of C15 NbCo₂. The hardness remains constant between 28 and 34 at.% Nb and decreases as the composition approaches the homogeneity ranges of the C14 and C36 variants. The decrease in hardness at off-stoichiometric compositions can be explained as an effect of the reduction in the Peierls stress. Whereas the hardness of C15 and C36 NbCo₂ is independent of orientation, C14 NbCo₂ shows slightly higher hardness values for the indentation orientation perpendicular to the basal plane.
- (2) Only few individual dislocations exist in C15 NbCo₂ in the composition range from 26 to 34 at.% Nb, whereas a high density of stacking faults were observed at the Co- and Nb-rich phase boundaries of C15 NbCo₂. The diffusion layers of C14 and C36 NbCo₂ also exhibit widely extended planar defects.
- (3) According to the calculation of the SFE as a function of composition, the formation of extrinsic stacking faults (i.e., C36-like) in C15 NbCo₂ is energetically more favorable than the formation of intrinsic stacking faults (i.e., C14-like) as the composition approaches the Co-rich phase boundary where C15 transforms to C36 NbCo₂. At the Nb-rich phase boundary, where the C15 structure transforms to C14, it is just the opposite

situation. The extrinsic SFE of C15 NbCo₂ decreases to 0 at 25 at.% Nb at 1200 °C, whereas the intrinsic SFE decreases to 4 mJ/m² at 34.3 at.% Nb at 1350 °C. The observed high density of stacking faults at the Co-rich and Nb-rich phase boundaries of C15 NbCo₂ is related to the low SFE at these compositions.

Methodology

To grow diffusion layers of the C14, C15, and C36 NbCo₂ Laves phases with sufficiently large thickness and grain size, two diffusion couples Co/Co–30Nb and Nb/Co–30Nb (in at.%), which are composed of pure Co, pure Nb, and a C15 NbCo₂ alloy with composition of 30 at.% Nb, were prepared. Details of their preparation are described in Ref. [34]. The Co/Co–30Nb and Nb/Co–30Nb diffusion couples were heat-treated at 1200 °C for 96 h and 1350 °C for 24 h, respectively. The heat treatments were performed in an argon atmosphere. After heat treatment, the diffusion couples were furnace-cooled. Because of the similarities in the structure and bonding of the cubic and hexagonal NbCo₂ Laves phases, residual stresses caused by thermal expansion mismatch between the diffusion layers of the NbCo₂ Laves phase are expected to be negligible. To exclude the possibility that the defects and mechanical properties of the diffusion layers of the cubic and hexagonal NbCo₂ Laves phases are influenced by residual stresses, equilibrium alloys of the cubic and hexagonal NbCo₂ Laves phases with different compositions were also tested for comparison. A bulk NbCo₂ alloy with nominal composition of 25 at.% Nb that had been heat-treated at 1100 °C for 720 h [2] and four as-cast bulk NbCo₂ alloys with nominal composition of 26, 30, 33, and 36 at.% Nb prepared in house by Voß [6, 7] were used in the present work. The compositions and crystal structure types of these NbCo₂ alloys are listed in Table I.

The microstructures of the diffusion couples and the alloys were observed by optical microscopy (Carl Zeiss light optical microscope) and scanning electron microscopy (SEM; JEOL JSM 6490). The concentration profiles of the diffusion couples were measured by EPMA using a JEOL JXA 8100 instrument with pure Co and Nb as standards. Three scans with a step width of 1 μm were measured for each diffusion couple. The crystallographic grain orientations were determined by EBSD mappings in selected areas of the diffusion couples using an EDAX/TSL detector setup with a Hikari CCD camera and a JEOL JSM 6490 SEM.

Defects in the cubic and hexagonal NbCo₂ Laves phases at different compositions were studied by ECCI observations at various positions along the concentration gradients of the diffusion couples using a Zeiss Merlin SEM. For defect analysis, single grains of interest were brought into two-beam conditions, where only one set of lattice planes in the crystal is

TABLE I: Nominal compositions, compositions analyzed by EPMA, and phases determined by XRD of the NbCo₂ alloys used in this study. The NbCo₂ alloy with nominal composition of 25 at.% Nb was synthesized by Stein et al. [2]. The NbCo₂ alloys with nominal compositions of 26, 30, 33, and 36 at.% Nb stem from Refs. [6, 7]. The analyzed compositions and phases are as given in Refs. [2, 6, 7].

Nominal composition (at.% Nb)	Analyzed alloy composition (at.% Nb)	Phases
25	25.1 ± 0.2	C36
26	25.6 ± 0.3	C36 + C15
30	30.0 ± 0.6	C15
33	33 ± 1	C15
36	36.0 ± 0.4	C14

positioned close to their Bragg angle. If two-beam conditions are satisfied, an individual dislocation appears as a bright line on a dark background with a bright dot, indicating the intersection point with the sample surface and fading contrast with increasing depth below the surface. A stacking fault appears as a bright area of a triangular or trapezoidal shape limited by a straight bright line that indicates the intersection of the stacking fault plane with the sample surface. The contrast of the stacking fault vanishes into the volume owing to the decreasing backscattering yield with increasing depth [10].

Nanoindentation testing was performed on both the diffusion couples and the alloys with a Berkovich indenter using an Agilent G200 nanoindenter at a maximum load of 40 mN. The indentation tests were performed at a constant loading rate of 2 mN/s and a hold time of 2 s. Oliver and Pharr's method [35] was used to determine the hardness and elastic modulus. The hardness H is calculated from the following equation:

$$H = \frac{P_{\max}}{A}, \quad (6)$$

where P_{\max} is the maximum load and A is the contact area which can be deduced from a well-calibrated tip shape function. The effective elastic modulus E_{eff} is calculated from the contact area and the unloading stiffness through the relation:

$$S = \beta \frac{2}{\sqrt{\pi}} E_{\text{eff}} \sqrt{A}, \quad (7)$$

where β is a constant with a value of 1.034 for a Berkovich indenter and S is the measured stiffness of the upper portion of the unloading data. The elastic modulus of the specimen E is extracted from the effective elastic modulus E_{eff} using the following relation:

$$\frac{1}{E_{\text{eff}}} = \frac{1 - \nu^2}{E} + \frac{1 - \nu_i^2}{E_i}, \quad (8)$$

where E_i is the modulus of the indenter, and ν and ν_i are Poisson's ratio for the specimen and the indenter, respectively. The values $E_i = 1141$ GPa, $\nu_i = 0.07$, and $\nu = 0.282$ [35] are used in the calculations.

A series of indents were made in the diffusion zones of the cubic and hexagonal NbCo₂ Laves phases along the concentration gradients to study the influence of composition and crystal structure on the hardness and elastic modulus. To avoid the influence of the interface, the indents are at least 15 μm from phase boundaries and consecutive indents. A minimum of 15 indentation tests were performed for each composition. To study the influence of orientation on the hardness, nano-indentation testing was also performed on the NbCo₂ alloys in various orientations, and at least 30 indents were made for each orientation in each alloy. All indents were observed by SEM after testing to measure their distance to the interface and to check whether there are microcracks or pores around the indents. All hardness and elastic modulus values are presented with their corresponding standard deviations.

Acknowledgments

The authors would like to thank Leon Christiansen and Angelika Bobrowski for their help in metallographic preparation and observation, Katja Angenendt and Monika Nellessen for their help in the ECCI observations, and Prof. Sharvan Kumar for discussions. Financial support from the China Scholarship Council (CSC) (No. 201406370160) and International Max Planck Research School for Interface Controlled Materials for Energy Conversion (IMPRS-SurMat) is gratefully acknowledged.

References

1. J.D. Livingston: Laves-phase superalloys? *Phys. Status Solidi A* **131**, 415 (1992).
2. F. Stein, D. Jiang, M. Palm, G. Sauthoff, D. Grüner, and G. Kreiner: Experimental reinvestigation of the Co–Nb phase diagram. *Intermetallics* **16**, 785 (2008).
3. C.T. Liu, J.H. Zhu, M.P. Brady, G.G. Mckamey, and L.M. Pike: Physical metallurgy and mechanical properties of transition-metal Laves phase alloys. *Intermetallics* **8**, 1119 (2000).
4. J.H. Zhu, L.M. Pike, C.T. Liu, and P.K. Liaw: Point defects in binary Laves phase alloys. *Acta Mater.* **47**, 2003 (1999).
5. S. Voß, F. Stein, M. Palm, D. Grüner, G. Kreiner, G. Frommeyer, and D. Raabe: Composition dependence of the hardness of Laves phases in the Fe–Nb and Co–Nb systems. *Mater. Res. Soc. Symp. Proc.* **1128**, 469 (2008).
6. S. Voß, F. Stein, M. Palm, and D. Raabe: Synthesis of defect-free single-phase bars of high-melting Laves phases through modified cold crucible levitation melting. *Mater. Sci. Eng., A* **527**, 7848 (2010).
7. S. Voß: Crystal structure and composition of the Fe–Nb(–Al) and Co–Nb systems. Doctoral thesis, RWTH Aachen University, Shaker Verlag, Aachen, Germany, 2010.

8. **K.C. Chen, F. Chu, P.G. Kotula, and D. Thoma:** HfCo₂ laves phase intermetallics—Part II: Elastic and mechanical properties as a function of composition. *Intermetallics* **9**, 785 (2001).
9. **J.-C. Zhao:** A combinatorial approach for efficient mapping of phase diagrams and properties. *J. Mater. Res.* **16**, 1565 (2001).
10. **S. Zaefferer and N-N. Elhami:** Theory and application of electron channelling contrast imaging under controlled diffraction conditions. *Acta Mater.* **75**, 20 (2014).
11. **A.V. Kazantzis, M. Aindow, I.P. Jones, G.K. Triantafyllidis, and J.T.M. De Hosson:** The mechanical properties and the deformation microstructures of the C15 Laves phase Cr₂Nb at high temperatures. *Acta Mater.* **55**, 1873 (2007).
12. **H. Kubsch, P. Paufler, and G.E.R. Schulze:** On the comparison between grown-in and fresh dislocations in the intermetallic compound MgZn₂. *Phys. Status Solidi A* **24**, K53 (1974).
13. **N. Takata, H. Ghassemi-Armaki, M. Takeyama, and S. Kumar:** Nanoindentation study on solid solution softening of Fe-rich Fe₂Nb Laves phase by Ni in Fe–Nb–Ni ternary alloys. *Intermetallics* **70**, 7 (2016).
14. **D.E. Luzzi, G. Rao, T.A. Dobbins, and D.P. Pope:** Deformation twinning at low temperatures in a Hf–V–Nb cubic laves phase. *Acta Mater.* **46**, 2913 (1998).
15. **P.M. Hazzledine, K.S. Kumar, D.B. Miracle, and A.G. Jackson:** Synchroshear of laves phases. *Mater. Res. Soc. Symp. Proc.* **288**, 591 (1992).
16. **L. Ma, T-W. Fan, B-Y. Tang, L-M. Peng, and W-j. Ding:** Ab initio study of I₂ and T₂ stacking faults in C14 Laves phase MgZn₂. *Eur. Phys. J. B* **86**, 188 (2013).
17. **F. Chu, A.H. Ormeci, T.E. Mitchell, J.M. Wills, D.J. Thoma, R.C. Albers, and S.P. Chen:** Stacking fault energy of the NbCr₂ Laves phase. *Philos. Mag. Lett.* **72**, 147 (1995).
18. **J. Sun and B. Jiang:** Ab initio calculation of the phase stability, mechanical properties and electronic structure of ZrCr₂ Laves phase compounds. *Philos. Mag.* **84**, 3133 (2004).
19. **C. He, F. Stein, and M. Palm:** Thermodynamic description of the systems Co–Nb, Al–Nb and Co–Al–Nb. *J. Alloys Compd.* **637**, 361 (2015).
20. **D. Grüner, F. Stein, M. Palm, J. Konrad, A. Ormeci, W. Schnelle, Y. Grin, and G. Kreiner:** Preparation, phase stability and structure of the C36 Laves phase Nb_{1–x}Co_{2+x}. *Z. Kristallogr.* **221**, 319 (2006).
21. **S. Chen, Y. Sun, Y-H. Duan, B. Huang, and M-J. Peng:** Phase stability, structural and elastic properties of C15-type Laves transition-metal compounds MCo₂ from first-principles calculations. *J. Alloys Compd.* **630**, 202 (2015).
22. **T. Müller and P. Paufler:** Yield strength of the monocrystalline intermetallic compound MgZn₂. *Phys. Status Solidi A* **40**, 471 (1977).
23. **P. Paufler:** Early work on laves phases in East Germany. *Intermetallics* **19**, 599 (2011).
24. **T. Takasugi, M. Yoshida, and S. Hanada:** Deformability improvement in C15 NbCr₂ intermetallics by addition of ternary elements. *Acta Mater.* **44**, 669 (1996).
25. **Y. Nakagawa, T. Ohta, Y. Kaneno, H. Inoue, and T. Takasugi:** Defect structures and room-temperature mechanical properties of C15 Laves phases in Zr–Nb–Cr and Zr–Hf–Cr alloy systems. *Metall. Mater. Trans. A* **35**, 3469 (2004).
26. **A.V. Kazantzis, M. Aindow, G.K. Triantafyllidis, and J.T.M. De Hosson:** On the self-pinning character of synchro-Shockley dislocations in a Laves phase during strain rate cyclical compressions. *Scr. Mater.* **59**, 788 (2008).
27. **P.M. Hazzledine and P. Pirouz:** Synchroshear transformation in Laves phases. *Scr. Metall. Mater.* **28**, 1277 (1993).
28. **X. Qiu, Y. Huang, W.D. Nix, K.C. Hwang, and H. Gao:** Effect of intrinsic lattice resistance in strain gradient plasticity. *Acta Mater.* **49**, 3949 (2001).
29. **K. Durst, B. Backes, O. Franke, and M. Göken:** Indentation size effect in metallic materials: Modeling strength from pop-in to macroscopic hardness using geometrically necessary dislocations. *Acta Mater.* **54**, 2547 (2006).
30. **W.D. Nix and H. Gao:** Indentation size effects in crystalline materials: A law for strain gradient plasticity. *J. Mech. Phys. Solids* **46**, 411 (1998).
31. **L. Liu, P. Shen, X. Wu, R. Wang, W. Li, and Q. Liu:** First-principles calculations on the stacking fault energy, surface energy and dislocation properties of NbCr₂ and HfCr₂. *Comput. Mater. Sci.* **140**, 334 (2017).
32. **J.N. Wang:** A new modification of the formulation of Peierls stress. *Acta Mater.* **44**, 1541 (1996).
33. **J.N. Wang:** Prediction of Peierls stresses for different crystals. *Mater. Sci. Eng., A* **206**, 259 (1996).
34. **W. Luo, C. Kirchlechner, X. Fang, S. Brinckmann, G. Dehm, and F. Stein:** Influence of composition and crystal structure on the fracture toughness of NbCo₂ Laves phase studied by micro-cantilever bending tests. *Mater. Des.* **145**, 116 (2018).
35. **W.C. Oliver and G.M. Pharr:** Measurement of hardness and elastic modulus by instrumented indentation: Advances in understanding and refinements to methodology. *J. Mater. Res.* **19**, 3 (2004).